SPECIAL ISSUE ARTICLE

The Anatomical Record
Advances in Integrative Anatomy and Evolutionary Biology
WILEY

From head to hind: Elucidating function through contrasting morphometrics of ancient and modern pedigree dogs

Jeffrey J. Schoenebeck[1,2] | Sheila Hamilton-Dyer[3] | Ian L. Baxter[4] |
Tobias Schwarz[2] | Marc Nussbaumer[5]

[1]Roslin Institute, The University of Edinburgh, Easter Bush, Midlothian, UK

[2]Royal (Dick) School of Veterinary Studies, The University of Edinburgh, Easter Bush, Midlothian, UK

[3]Bournemouth University, Poole, Dorset, UK

[4]Coalville, Leicestershire, UK

[5]Naturhistorisches Museum, Bern, Switzerland

Correspondence
Jeffrey J. Schoenebeck, Roslin Institute, The University of Edinburgh, Easter Bush, Midlothian EH25 9RG, UK.
Email: jeff.schoenebeck@roslin.ac.ed.uk

Marc Nussbaumer, Naturhistorisches Museum, Bernastrasse 15, Bern CH-3005, Switzerland.
Email: marc.nussbaumer@nmbe.ch

Abstract

Used together, caliper- and geometric-based morphometric analyses provide complimentary approaches to classifying form and function of archaeozoological remains. Here we apply these analytical tools to the skeletal remains of an ancient male dog unearthed from a rural farm settlement of Roman date near present day Warmington, United Kingdom. Our comparisons of the Warmington Roman dog against the morphological characteristics of modern dog breeds enabled us to establish the former's size and shape. It was of medium stature. Analysis of viscerocrania and neurocrania indicate it falls within the meso- to dolichocephalic rankings of modern dogs. The neurocranium shape and the dimensions of its long bones strongly suggest that the Warmington dog shares similarities to modern sight hounds. Historically sight hounds were bred for speed, as necessitated of a hunter that runs down small prey. Our analysis suggests that the Warmington dog was likely bred for, or derived from, Roman hunting stock. By revealing the Warmington Roman dog's form from cranial and postcranial analyses, we shed light on Roman life in one of the furthest outposts of the Roman Empire.

KEYWORDS

archaeozoology, dog, geometric morphometrics, morphology, Roman

1 | INTRODUCTION

Based on morphological data and molecular evolution estimates, dogs were probably domesticated from one or more extinct lineages of wolves at least 15,000 years before present (Botigué et al., 2017; Frantz et al., 2016; Freedman et al., 2014; Pionnier-Capitan et al., 2011; Skoglund, Ersmark, Palkopoulou, & Dalén, 2015; Wang et al., 2013). Ironically, the breadth of morphotypes of present-day dogs belies the fact that their diversity is due to the selective breeding practices of Victorian-era dog fanciers. During the 19th century, fanciers bred for specializations including hunting, guarding, drafting, herding, vermin-control and companionship. The formation of clubs like the Kennel Club and American Kennel Club, whose bylaws standardized both dog

forms and their propagation, formalized dog breeds as we know them today.

Dogs of antiquity also varied in morphology, though these were landraces rather than breeds. Classic literature suggests that the Roman province of Britannia (Great Britain) was renowned for its hunting and war dogs, which it exported (Smith, 2005). Among the better-known Romano-British excavation sites, Calleva Atrebatum and Vindolanda have yielded large collections of dog skeletal remains (Bennett, Cambell, & Timm, 2016; Bennett & Timm, 2016; Lobell & Powell, 2010). Analyses of individual bones suggest that the dogs produced by Britannia were morphologically diverse (Bennett et al., 2016; Harcourt, 1974).

Here we utilized linear distances and geometric morphometrics, as well as pathological analysis, to infer from skeletal remains the life and purpose of a Romano-British dog unearthed near Warmington (Warwickshire, England, United Kingdom). The exceptional preservation of this dog's cranial and postcranial bones afforded a "systems-level" comparison of it to modern canine breed morphotypes.

2 | MATERIALS AND METHODS

2.1 | Archaeological site and dating

The excavations by the Warmington Heritage Group at Warmington, Warwickshire, are on the edge of the north Cotswold escarpment, overlooking the Feldon Valley (Figure 1a). Roman settlement and religious activities were preceded by a prehistoric burial and a massive Iron Age ditch and bank.

The principal excavation area revealed a sequence of five nondomestic buildings, probably spanning the whole of the period of the Roman occupation. The exact functions of these buildings remain unclear, though it is believed that they supported a peasant farm as well as iron smithing. Two hoards of denarii were uncovered that dated after the conquest of Britain, the most recently minted coin from 70CE. Based on dated soil strata that included pottery fragments, tile, and metal works, it is assumed the farm was in use around the third quarter of the first century CE.

FIGURE 1 Location of the Warmington Roman dog. Google Maps depicting the location of Warmington, Warwickshire, United Kingdom (pin drop, a). Dog remains in situ (b). Skull images including dorsal (c), ventral (d), lateral right (e), and lateral left (f). Size bar indicates 5 cm distance. Image credits: Marc Nussbaumer

In addition to these materials, burials of two dogs and an eagle skeleton were unearthed. The incomplete skeletal remains of a small dog, which was disturbed by modern ploughing, were provisionally dated to the aforementioned Roman period.

The larger dog, whose morphology is described in detail here, consists of a complete, articulated skeleton that appears to have been deliberately laid to rest on its right side. A baculum was recovered, indicating it was a male. It was found in a pit, 1.5 m wide and 1.3 m deep. The pit fill contained animal bones, pottery and building rubble. The contents of the pit had settled and some of the dog's joints had slightly separated as a result (Figure 1b). The rubble matrix made lifting the dog in a block impractical, so it was excavated and recorded bone by bone over several weeks. The skull and the pelvic area were lifted in blocks for excavation in the laboratory. There were no signs of mortal injuries, cut marks, or signs of disassembly. Based on these observations, the dog is believed to have been deliberately buried rather than disposed of with general waste.

2.2 | Museum specimens

The skeletal remains of modern breed dogs used in our study are housed as part of the Natural History Museum of Bern (NMBE)'s Albert Heim world-leading canine collection. All skeletons analyzed by landmarks or measurements were from adults >24 month old ($N = 116$, 52 males, 64 females) which were donated to the museum by owners. Breed identity was confirmed by pedigree and genetic analysis (JJS, data not shown). All dogs were intact (unneutered) at time of death. The skulls of 114 dogs were landmarked for geometric morphometric analysis. Sixty-three of these had accompanying postcranial bones that were measured. Two dogs that had postcranial skeletons, but not skulls, were also measured.

2.3 | Landmarks and measurements analysis

Landmarks were captured using a MicroScribe® digitizer (model MX, 6DoF) attached to a laptop running Microsoft Window XP and the Microscribe Utility Software (v6.0). The 51 landmarks chosen for analysis were previously described by Schoenebeck et al. (2012). We used subsets of the 51 landmarks to define shapes of viscerocrania and neurocrania in isolation (Table 1). The Warmington Roman dog skull was damaged particularly along the right proximal nasal bone and

zygomatic arch. For the nasal bone, we estimated the position of missing data by reflecting symmetric Procrustes coordinates from left mediolateral landmarks (see next paragraph). The position of nasion landmarks along the rostral leading edge were estimated using a bridge fashioned from masking tape. Landmarks located on the right zygomatic arch were captured after reassembling the right zygomatic arch which had been broken off as a single fragment. Raw and Procrustes coordinates are provided in Tables S1 and S2. These large tables are freely accessible within the University of Edinburgh's DataShare digital repository (https://doi.org/10.7488/ds/2538).

Most skulls were landmarked once, while the Warmington Roman dog skull was landmarked three times. The coordinate system of the Microscribe was calibrated locally for x-, y-, and z-axes. Landmarks were recorded in millimeters. Raw coordinates were imported into Microsoft Excel for Mac 2011 (v14.6.4). Coordinate data were exported as a text file, reformatted using a custom R script, and imported into MorphoJ (v1.06c) where a general Procrustes fit was applied to the covariance matrix. A by-product of the fit is the centroid size, a proxy for scale (Table S2). In our study, we used individual centroid sizes of the neurocranium to estimate animal size. In order to minimize the effects of allometry, the covariance matrix of symmetric Procrustes coordinates was regressed against the centroid size. A second symmetric matrix of distances from individuals in multidimensional space was generated from the residuals of this regression. Principal components analysis (PCA), an ordination method that decomposes the covariances into components of successively smaller, uncorrelated eigenvectors, were used to assess specimens' position in morphospace. To avoid over plotting, the bivariate plots depict breed averages of the components. We restricted our consideration of skull shape to PC1 and PC2. The angle between the hard palate and skull base ("β angle," see Nussbaumer, 1982) was calculated from landmark data using a custom R script.

We selected 14 postcranial measurements for analysis (Table 2, Table S2) (von den Driesch, 1976). Measurements were collected by digital calipers hardwired to a Microsoft Windows desktop. Measurements were collected in millimeters and imported directly into Microsoft Excel (v14.0.7177). All postcranial measurements were taken twice and averaged (Table S2). To reduce allometric effects on shape, individual size was defined as the geometric mean. Each subject's measurements were divided by its size and log transformed to generate log-shape ratios

TABLE 1 Description of landmarks

Landmark name	Whole skull	Neurocranium	Viscerocranium
P_hirnstammbasis	X	X	
Opsithion	X	X	
Lambda	X	X	
Bregma	X	X	
Nasion	X		X
Nasale	X		X
Intradental_superior	X		X
Premax_max_junct_at_alveolus_R	X		X
Premax_max_junct_at_alveolus_L	X		X
Nasal_premaxillary_at_external_naris_R	X		X
Nasal_premaxillary_at_external_naris_L	X		X
Maxilla_frontal_nasal_junct_R	X		X
Maxilla_frontal_nasal_junct_L	X		X
Premax_max_nasal_junct_R	X		X
Premax_max_nasal_junct_L	X		X
R_infraorbital_dorsal	X		X
L_infraorbital_dorsal	X		X
R_infraorbital_ventral	X		X
L_infraorbital_ventral	X		X
Frontal_maxillary_lacrimal_junct_R	X		X
Frontal_maxillary_lacrimal_junct_L	X		X
Frontal_lacrimal_palantine_junct_R	X		X
Frontal_lacrimal_palantine_junct_L	X		X
Ethmoid_foramen_dorsal_R	X	X	
Ethmoid_foramen_dorsal_L	X	X	
Pterion_anterior_R	X	X	
Pterion_anterior_L	X	X	
Pterion_posterior_R	X	X	
Pterion_posterior_L	X	X	
Zygomaxillar_dimple_R	X		X
Zygomaxillar_dimple_L	X		X
Premolar_to_molar_R	X		X
Premolar_to_molar_L	X		X
Superior_postorbital_process_R	X		
Superior_postorbital_process_L	X		
Inferior_postorbital_process_R	X		X
Inferior_postorbital_process_L	X		X
Nuchal_Crest_Flare_R	X	X	
Nuchal_Crest_Flare_L	X	X	
Asterion_R	X	X	
Asterion_L	X	X	
Hirnstammbasis_Anterior	X	X	
Posterior_nasal_spine	X		X
Maxillary_palantine_at_midline	X		X
Premaxilary_maxillary_at_midline_palate	X		X
Temporal_jugal_junction_R	X		
Temporal_jugal_junction_L	X		
Foramen_ovale_R	X	X	
Foramen_ovale_L	X	X	
Hypoglossal_canal_R	X	X	
Hypoglossal_canal_L	X	X	

TABLE 2 Caliper measurements and Harcourt height estimates

Name	Description or formula	Measurement (mm)	Used in this study?	Reference
Estimated height at withers (humerus)	=3.43*HUMERUS_GLC	616	Yes	Harcourt (1974)
Estimated height at withers (radius)	=3.18*RADIUS_GL	601	Yes	Harcourt (1974)
Estimated height at withers (humerus + radius)	=1.65*(HUMERUS_GLC + RADIUS_GL) − 4.32	604	Yes	Harcourt (1974)
Estimated height at withers (femur)	=3.14*FEMUR_GLC	638	Yes	Harcourt (1974)
Estimated height at withers (tibia)	=2.92*TIBIA_GL	626	Yes	Harcourt (1974)
Estimated height at withers (femur + tibia)	=1.52*(FEMUR_GLC + TIBIA_GL) − 2.47	632	Yes	Harcourt (1974)
B	Length of skull base from back of Incisiva1 to front of foramen magnum	176	No	Lüps (1973)
C	From the front of the foramen magnum to the suture palatine/maxilla	111	No	Lüps (1973)
D	Front of the foramen magnum to the suture pterygoid/palatinum where the palatinum meets the presphenoid	62	No	Lüps (1973)
F	Width over the canines	37	No	Lüps (1973)
G	Largest width over zygomatic (cranial width)	104	No	Lüps (1973)
H	Width over retroarticular processes	50	No	Lüps (1973)
M	Caudal zone of palatine	34	No	Lüps (1973)
BETA	Angle between skull base and hard palate	176	Yes	Lüps (1973)
SACRUM_GB	Sacrum greatest breadth	49	Yes	von den Driesch (1976)
SACRUM_PL	Sacrum physiological length	36	Yes	von den Driesch (1976)
PELVIS_GL	Pelvis greatest length	162	Yes	von den Driesch (1976)
PELVIS_GBA	Pelvis greatest breadth across acetabula	83	Yes	von den Driesch (1976)
HUMERUS_GLC	Humerus greatest length from caput	180	Yes	von den Driesch (1976)
HUMERUS_BD	Humerus greatest breadth distal end	36	Yes	von den Driesch (1976)
HUMERUS_SD	Humerus smallest diameter	14	Yes	von den Driesch (1976)
RADIUS_GL	Radius greatest length	189	Yes	von den Driesch (1976)
RADIUS_SD	Radius smallest diameter	7	Yes	von den Driesch (1976)
FEMUR_GLC	Greatest length from caput femoris	203	Yes	von den Driesch (1976)
FEMUR_SD	Femur smallest diameter	13	Yes	von den Driesch (1976)
TIBIA_GL	Tibia greatest length	214	Yes	von den Driesch (1976)
TIBIA_BP	Tibia greatest breadth of proximal end	36	Yes	von den Driesch (1976)
TIBIA_SD	Tibia smallest diameter	12	Yes	von den Driesch (1976)

(Mosimann, 1970). Log-shape ratios were converted to a distance matrix and analyzed by PCA.

To facilitate rapid comparison of the Warmington Roman dog with other studies, we provided basic measurements described by Lüps (1973), Harcourt (1974), and von den Driesch (1976) and in Table 2.

Data analysis and plotting data were generated in RStudio (v1.1.456) running R version 3.5.1 (2018-07-02).

Packages used in our study included FactoMineR (1.4.1), ggplot2 (v3.1.0), and reshape2 (v1.4.3) packages.

2.4 | Skull images

Comparative images of the Warmington Roman dog and other museum specimens were captured on a Panasonic Lumix digital camera (DMC-FZ1000) outfitted with a Leica DC Vario-Elmarit 1:2.8-4/9.1–146 mm ASPH.

2.5 | Diagnostic imaging

Computed tomography was performed on the Warmington Roman dog skeletal remains using a helical 4-slice CT unit (Somatom Volume Zoom, Siemens, Germany). The scans consisted of 1 mm slice width series of the head and selected postcranial bones. CT settings included 120 kV tube voltage, 93–134 mA adaptive tube current, 1.5 s tube rotation time, 207–362 mm display field of view diameter and 512^2 image matrix. Images were reconstructed into DICOM format with an image reconstruction kernel for bone (Siemens proprietary name H70h).

All CT studies were retrospectively reviewed for skeletal abnormalities by a board-certified veterinary radiologist (T. Schwarz), who was not aware of the disease status of the animal at the time of evaluation. Images were evaluated using dedicated DICOM viewer software (OsiriX, Geneva, Switzerland, version 5.8.5-64bit) on a computer workstation (Mac Pro, Apple) with a calibrated LCD flat screen monitor (Thunderbolt Display, 27-in., Apple). During the course of image evaluation, multi-planar reconstructions and variable windowing were used according to the preferences of the viewer. Standard anatomic and diagnostic imaging references were used for the evaluation (Mihaljević, Kramer, & Gomerčić, 2009; Schwarz & Saunders, 2011).

2.6 | Data availability

Archaeological reports and data used in this study are made available through the University of Edinburgh's DataShare digital repository (https://doi.org/10.7488/ds/2538).

3 | RESULTS

3.1 | Whole skull

We compared the Warmington Roman dog skull to those of modern breed dogs. Given the tremendous size variation between modern dog breeds, we removed allometry and focused on shape ordination defined by principal components analysis (see Section 2 for details). This decision was supported by the observation that retention of allometry in principal components analysis resulted in a single, loosely clustered group of morphologically "moderate" skulls, including that of the Warmington Roman dog (data not shown).

PC1 (66.3% variance) explained facial retrusion, lateral expansion of the zygoma, and height of the sagittal crest. Breeds with positive PC1 values are dolichocephalic ("long-headed"), such as the Borzoi, Scottish Terrier, and Dachshund. Judged by PC1, the Warmington Roman dog was mesocephalic (Figure 2, Table S3).

Examination of landmark vectors indicates that PC2 describes differences in the hard palate angle with respect to the skull base and height of the sagittal crest. The Warmington Roman dog established the negative boundary of PC2 (4.9% variance): its hard palate extends parallel to the skull base (Figure 2, Table S3) and the location of its frontal-nasal-maxilla junction is more caudal with respect to the other dogs (Figure 3). These features are not well represented among the skulls of modern dogs we surveyed, thus explaining why the Warmington Roman dog skull appears as an outlier with respect to PC2.

3.2 | Facial skeleton and neurocranium

Previous works suggested modularity between the facial skeleton and the neurocranium (Drake & Klingenberg, 2010; Parr et al., 2016). This observation, as well as the disparate developmental origins of these two regions of the skull in amniotes, prompted us to treat their morphological analysis separately (Jiang, Iseki, Maxson, Sucov, & Morriss-Kay, 2002; McBratney-Owen, Iseki, Bamforth, Olsen, & Morriss-Kay, 2008; Noden & Trainor, 2005). Focusing on 28 landmarks located on the viscerocranium to the neurocranium, we observed that facial skeleton (fs) PC1 defined the axis of facial retrusion/protrusion, accounting for 72% of variance. fsPC2 (4.9% variance) was driven by coefficients corresponding to subtle positional shifts in the frontal-nasal-maxilla junction (Figure 3, Table S3). In terms of its place within morphospace, the facial skeleton of the Warmington Roman dog is somewhat unusual with respect to the modern dog breeds we compared it against: while its fsPC1 value ranks it among modestly dolichocephalic breeds including the Schwyz Hound and Belgian Tervuren, the dorsocaudal shift of the frontal-nasal-maxillary junctions underpins PC2
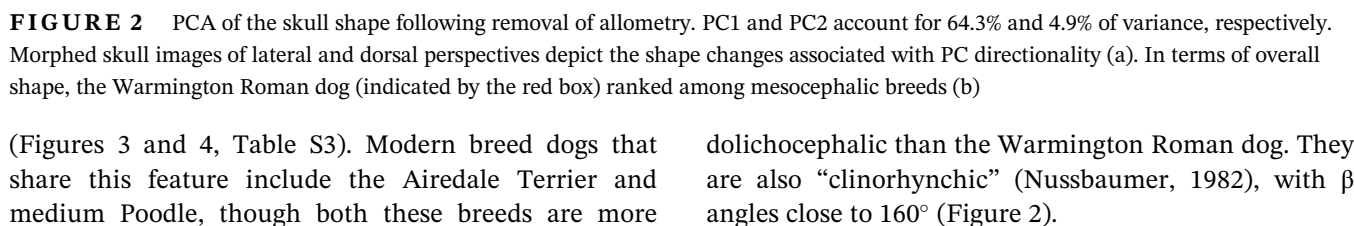
FIGURE 2 PCA of the skull shape following removal of allometry. PC1 and PC2 account for 64.3% and 4.9% of variance, respectively. Morphed skull images of lateral and dorsal perspectives depict the shape changes associated with PC directionality (a). In terms of overall shape, the Warmington Roman dog (indicated by the red box) ranked among mesocephalic breeds (b)

(Figures 3 and 4, Table S3). Modern breed dogs that share this feature include the Airedale Terrier and medium Poodle, though both these breeds are more dolichocephalic than the Warmington Roman dog. They are also "clinorhynchic" (Nussbaumer, 1982), with β angles close to 160° (Figure 2).

FIGURE 3 Comparison of the Roman Warmington dog to historic and modern sight hound skulls. From left to right, top row: two Greyhounds (1980s); middle row: Greyhound (Bern ca. 1900), Warmington Roman dog, Greyhound (Bern, ca. 1900); and bottom row: four "Windhund" (Berlin, ca. 1800). Note the relative positions of the intersection between frontal, maxilla, and nasal bones as indicated by arrowheads. The intersection of these bones is comparatively caudal in the Warmington Roman dog (red arrowhead) Image credit: Marc Nussbaumer

Our analysis of the neurocranium (nc) included 19 landmarks (Table 1), avoiding the facial skeleton, zygomatic arches, and sinuses. Despite controlling for allometry, ncPC1 remains correlated with centroid size (adjusted $R^2 = 0.86$, data not shown). This is because features of the cranial vault, such as the attachment points of tendons associated with jaw and neck muscles, are pronounced in dogs that were bred to meet physical demands requiring speed and power. Such dogs are inevitably medium, large and giant in size, with St. Bernard and Leonberger occupying the positive pole of the ncPC1 continuum (Figure 5a,b, Table S3). Conversely, toy and small dogs such as the Chihuahua, occupy the negative pole of PC1. These dogs lack pronounced sagittal and nuchal crests, the attachment points for the temporalis muscles (Figure 5a). ncPC2 (12.4% variance) describes length and width of the neurocranium and is negatively correlated with fsPC1 (i.e., facial skeleton length, adjusted $R^2 = 0.5$). In general, dogs with short faces have spheroid-shaped vaults. Conversely, dogs with longer faces such as the borzoi have neurocrania that are elongated along the rostrocaudal axis (Drake, 2011; Marchant

et al., 2017; Schoenebeck et al., 2012; Selba, Oechtering, Heng, & DeLeon, 2019). The Warmington Roman dog's positive ncPC1 and negative ncPC2 scores places it within morphospace that is also occupied by medium-sized herding or hunting dogs. Overall, its neurocranium shape was akin to that of a Belgian Shepherd, Airedale Terrier, Nova Scotia Duck Tolling Retriever, and Afghan and Podenco Hounds, while the centroid size of the neurocranium placed it somewhere between the Afghan and Podenco Hounds (Figure 5C).

3.3 | Morphological variance of the postcranial skeleton

Postcranial skeleton measurements were collected from 61 of the museum dogs used in the skull analysis and the Warmington Roman dog (Table S2). Postcranial skeleton data from two addition Chihuahuas (without skulls) were also included. Using Harcourt's factors on the four principal long bones (humerus, radius, femur, and tibia), we conclude that the Warmington Roman dog stood
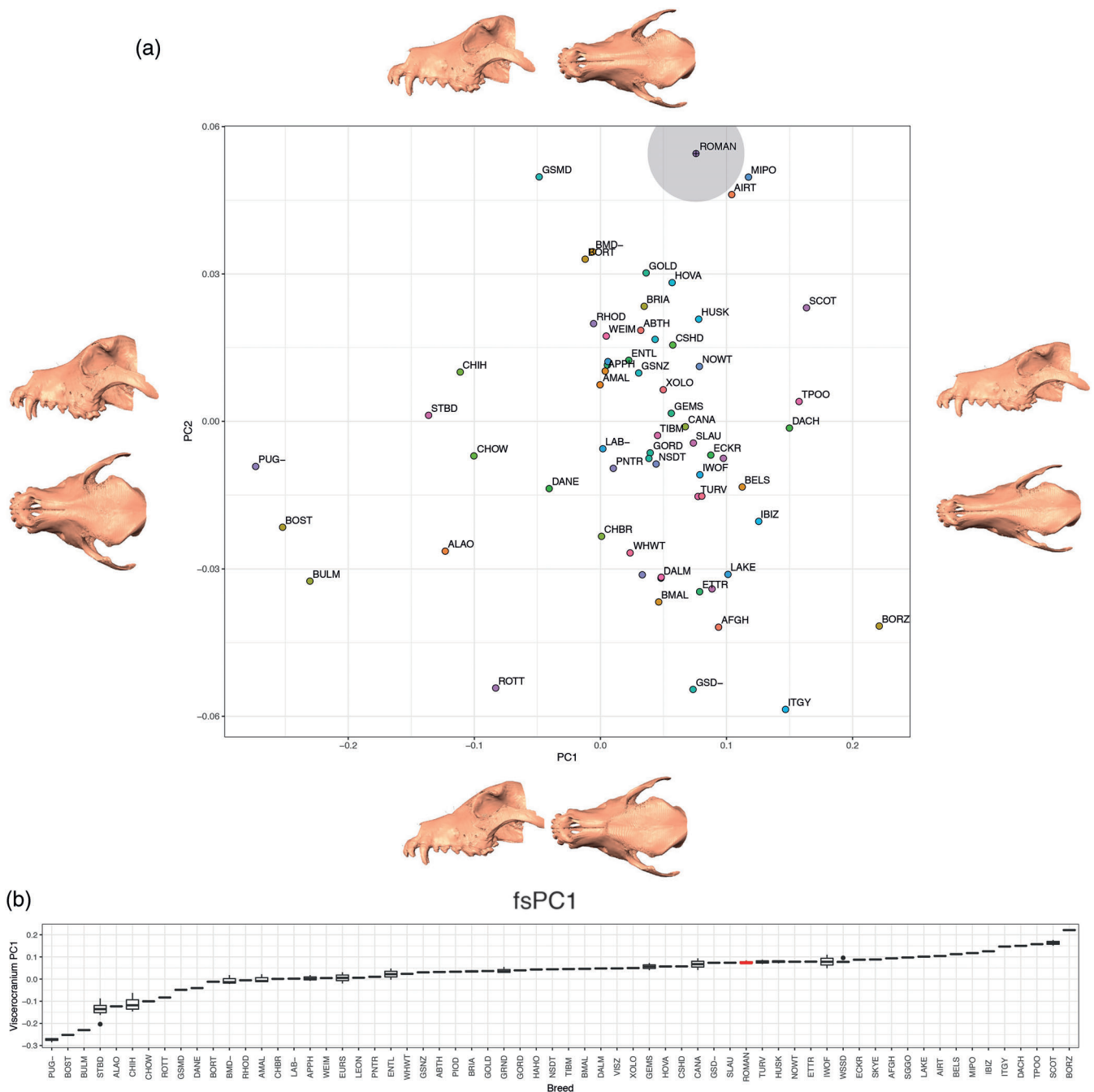
FIGURE 4 Facial skeleton shape without allometry. fsPC1 and fsPC2 account for 72.2% and 4.9% of variance, respectively. Morphed skull images of lateral and dorsal perspectives depict the shape changes associated with fsPC directionality (a). Boxplots of fsPC1 indicate that the Warmington Roman dog's face length (box marked in red) bridges meso- and dolicho-cephalic modern breed dogs (b)

between 61 and 63 cm at its withers (Table 2) (Harcourt, 1974). A distance matrix of 14 log-shape ratios (Mosimann, 1970) derived from bone measurements including the sacrum, pelvis, femur, tibia, humerus and radius were processed by principal component analysis (Figure 6, Table S3).

pocrPC1 explains 92.5% of the variance and is characterized by the trade-off between loadings corresponding to appendicular bone length and width, a phenomena

described in dogs previously (Figure 6, Table S3) (Chase et al., 2002). Chondrodysplastic breeds of dogs such as the Scottish Terrier, Norwich Terrier, and Chihuahua and to a lesser extent, large working breeds like the St. Bernard and Bernese Mountain Dog have disproportionately shorter and thicker long bones. Conversely, running and sprinting breeds such as the sight hounds have long, thin appendicular bones, as well as long, narrow pelvises. Interestingly, the lower limits of pocrPC1
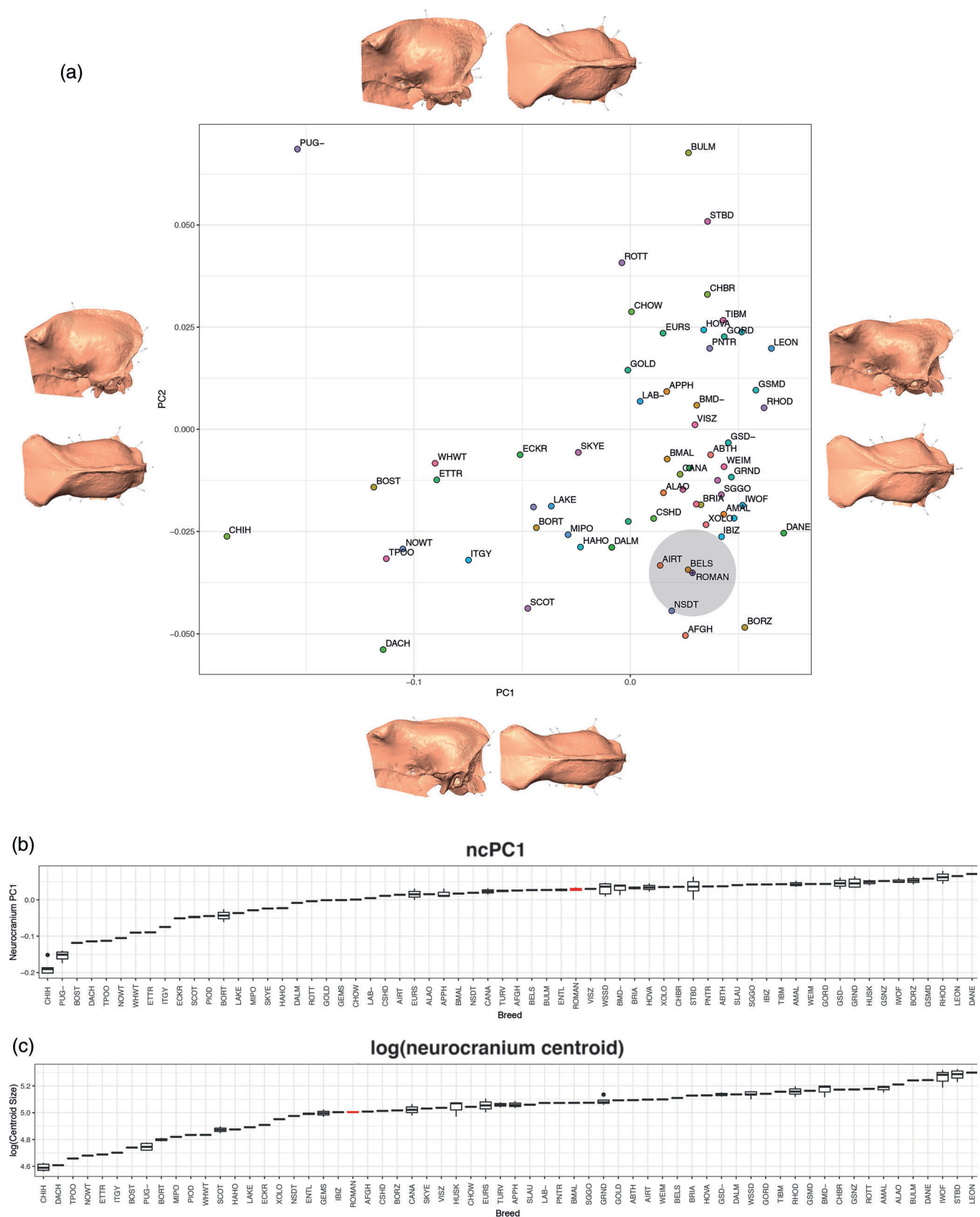
FIGURE 5 Size and shape of the neurocranium. PCA of shape, with allometry removed (a). PC1 and PC2 account for 44.5% and 12.4% of variance, respectively. Morphed skull images of lateral and dorsal perspectives depict the shape changes associated with PC directionality. Boxplots (b, c) of PC1 and neurocranium size (log[neurocranium centroid]), b and c. The neurocranium of the Warmington Roman dog was less ovoid and tapered more steeply along the rostrocaudal axis; its size was comparable to the Afghan and Podenco Hounds

FIGURE 6 Principal components analysis of the postcranial skeleton. Heatmaps of distance matrices generated from loadings of 14 measurements (a) and the PC values of dogs included in the analysis (b). Both maps were sorted by hierarchical clustering. PC values are centered, with zero indicated by the vertical aquamarine dashed line. The vertical aquamarine solid line indicates loadings or individual PC values, respective to the panels. In Panel (a), measurements are indicated in grey to indicate whether they are length-based (i.e., anteroposterior or proximal distal) or black to indicate they are width-based (mediolateral). In Panel (b), the Warmington Roman dog is indicated by the red arrowhead. Loadings are labeled by bone and measurement, where the latter corresponds as follows: greatest length from caput (GLC), greatest length (GL), smallest diameter (SD), greatest breadth proximal end (BP), greatest length distal end (BD), greatest breadth across the acetabula (GBA), greatest breadth across wings (GB). A comparison of the Warmington Roman dog long bones to that of an Afghan Hound (NMBE #1051205). Bones ordered in pairs (Afghan hound left, Warmington Roman dog right), left to right: femur, tibia, humerus, radius (c). Size bar corresponds to 10 cm

values are defined by the Warmington Roman dog and Afghan Hound, suggesting that the former was equipped for running (Figure 6c).

pocrPC2 explains 3.4% of the variance. Loadings particularly pertinent involve tradeoffs between shaft diameter and the distal breadth of long bones. This component separates giant and working breed dogs

from toy breeds, the Afghan Hound, and the Warmington Roman dog.

pocrPC3 (2% variance) showed sizeable intrabreed variability (data not shown). The Roman Warmington dog defines the positive limit of this PC, along with the Toy Poodle, Appenzell Cattle Dog, and Afghan Hound. They are opposed by breeds such as the White Swiss Shepherd
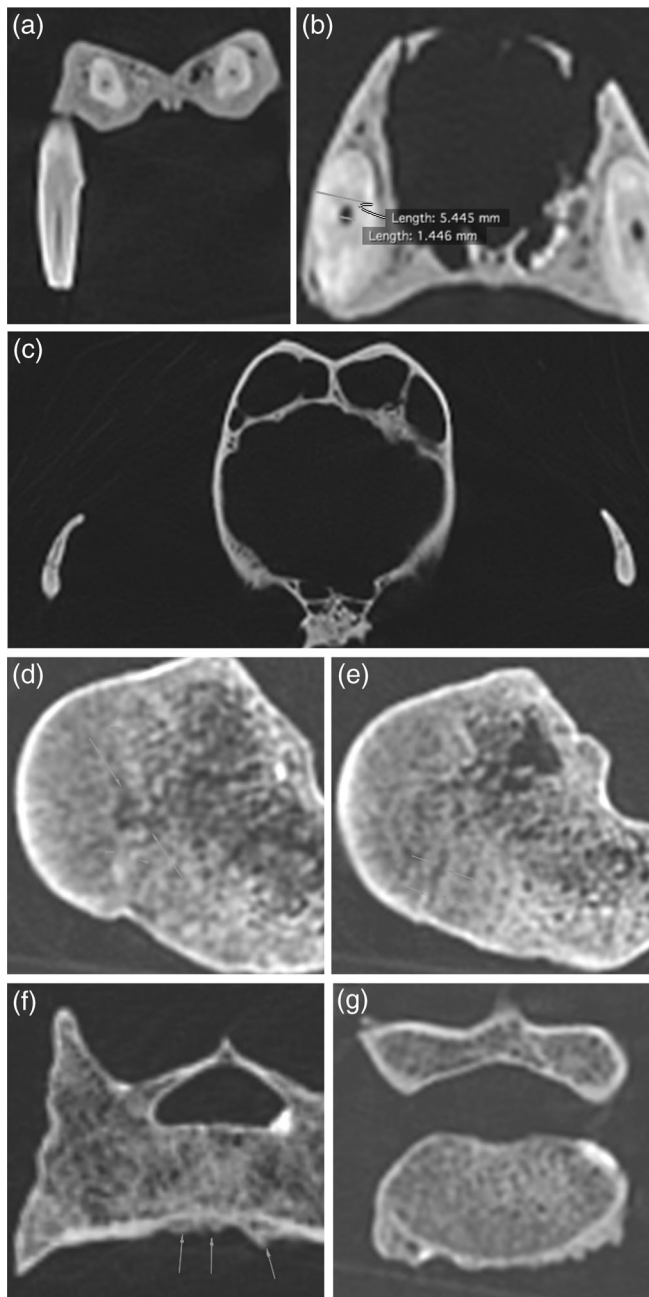
FIGURE 7 Clinical pathology of the Warmington Roman dog. CT slices (a–g). Anatomic right appears on the left side of images (a–c). Longitudinal section of the right maxillary canine (a). Cross section of the right maxillary canine (b). Cross section of the skull showing patent zygomaticotemporal sutures (c). Physeal scars, indicated by arrowheads, were observed within the proximal right humerus (d). Distal to these, a nonossified core breached the physis (e). Regions of incomplete ossification were observed in both sections (arrowheads). Irregular bone growth, indicated by arrows, was observed on ventral sides of both the sacrum (f) and L7 lumbar vertebrae (g)

and Border Terrier. The relationship between loadings and morphology is unclear for this PC, as well as for pocrPC4 and pocrPC5 (0.6% and 0.4% variance, respectively).

3.4 | Computed tomography

To examine the Warmington Roman dog bones in closer detail, the skeletal remains including the skull, vertebrae, and long bones of the appendicular skeleton were scanned by computed tomography and assessed for signs of aging and pathology.

We found numerous bone fractures visible with no evidence of a bony reaction. Within the cavities of the skull, several areas of mineral dense material are present which most likely represent soil.

The infradentale of the left mandible bearing the mandibular incisors is missing (data not shown). Apart from this, the specimen bears a complete set of permanent teeth according to the canine dental formula *I* 3/3, *C* 1/1, *P* 4/4, *M* 2/3. The 104 (right maxillary canine) and 404 (right mandibular canine) teeth have a small defect in its cusp with mineral dense material in the exposed pulp cavity (Figure 7a). Otherwise all teeth show intact cusps and enamel cover. The pulp cavities are relatively small, consistent with an adult dog (Figure 7b). The zygomaticotemporal suture is not bilaterally ossified (Figure 7c).
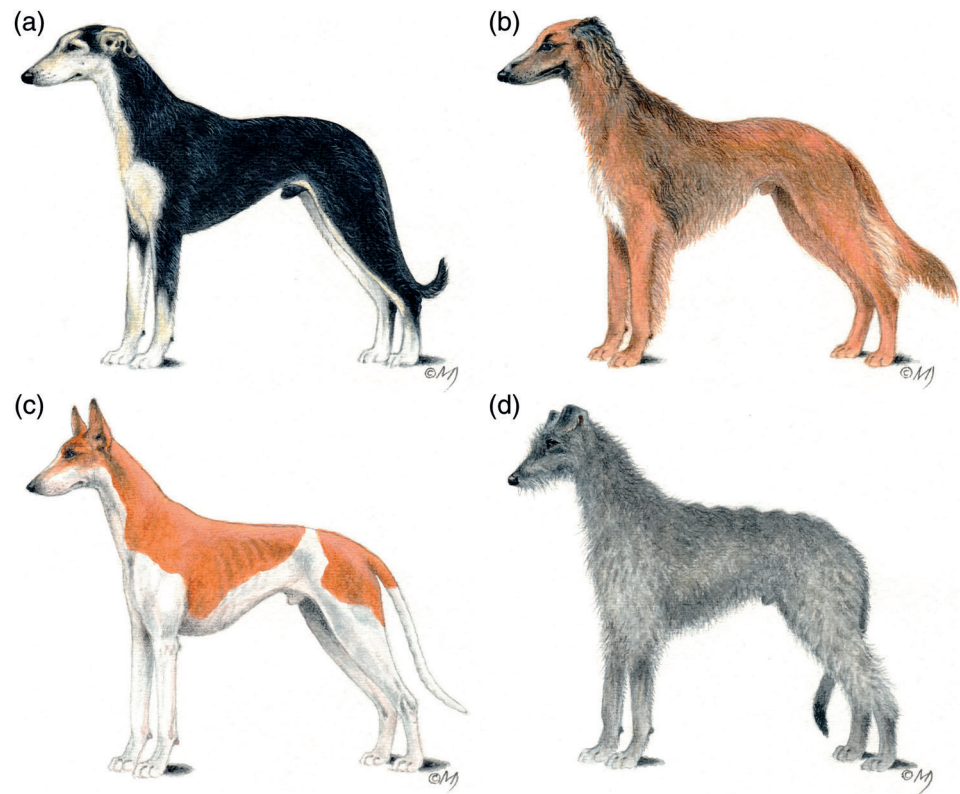
Bilaterally in the proximal humerus there is a discernible physeal scar (Figure 7d). In the right humerus there is a non-ossified core breaching the physis and a small peripheral area of non-fusion (Figure 7e). Bilaterally in the proximal femur there is a physeal scar and bilaterally in the tibia the proximal physis for tibial tuberosity is not fully ossified (data not shown). At the cranioventral aspect of the sacrum there is irregular bone formation with remodeling of the cortical bone (Figure 7f). Similar new bone formation is found on the caudoventral margin of the presumed L7 lumbar vertebra (Figure 7g).

4 | DISCUSSION

This study took a skeletal system wide approach to contrast the Warmington Roman dog with modern breed dogs. Analysis of the postcranial skeleton and to a lesser extent the neurocranium indicates its morphologically similar to modern sight hounds. In contrast, this dog was modestly dolichocephalic with no angle between its skull base and hard palate. Moreover, positioning of its frontal-nasal-maxilla junctions placed it on the edge of skull and facial skeleton morphospaces.

While geometric morphometric analysis of the skull enabled us to address separate scale from shape (Section 2), it was not practical to conduct a similar multivariate analysis on each of the six postcranial bones included in our comparisons. With the

FIGURE 8 Hypothetical appearances of the Warmington Roman dog. Illustrations considered the proportions of long bone and skull measurements, as well as the appearances of modern sight hounds. Coat length and texture, pigmentation, as well as ear and tail carriage diversify dogs' appearances. Overlaying these superficial differences to the gracile form of its skeleton transforms the appearance of the Warmington Roman dog. Artist: Maya Delaquis

availability of portable surface scanners and photogrammetric techniques (Evin et al., 2016), future work that applies a geometric morphometric analysis to the postcranial skeleton bones of this study's subjects might reveal additional differences.

4.1 | Growth effects and allometry

Our study has focused on intraspecies morphological variation, the basis of which is largely genetic. Scale, the largest source of dogs' morphological variation, is recognized to influence morphology (Drake & Klingenberg, 2010; Klingenberg, 2016; Wayne, 1986). As a single species, it is tempting to assume that shape differences due to allometry manifest similarly across dog breeds. However, size is a breed-defining feature that has been under stringent artificial selection for hundreds of years. The genetic variants that were selected to impart morphological diversification have large effect sizes (Boyko et al., 2010; Sutter et al., 2007). Moreover, variants that affect leg length such as the *FGF4* retrotransposon (Parker et al., 2009) are likely to be pleiotropic, affecting more than one aspect of the skeleton (Marchant et al., 2017). While progress has been made to identify genetic variants responsible for dogs' morphological disparities, integration of this information to model allometric effects is lagging. Such

studies will require individual level morphometrics, coupled with their genotypes to use as grouping criteria (Klingenberg, 2016).

4.2 | Pathology and age

Dental attrition and abrasion can cause wearing down of tooth surfaces and enamel cover. Dental attrition is defined as wearing down of tooth structures due to tooth-to-tooth contact, though it can also occur among dogs that have been provided a bone rich diet. The zygomaticotemporal suture is a late closing squamous suture for which exact closing dates have not been established in the dog, but radiographic evidence suggests that closure occurs between 38 and 52 weeks of age (Geiger & Haussman, 2016; Ryan, Fraga-Manteiga, Schwarz, & Clements, 2013). The proximal physes of the humerus, femur and tibial tuberosity have published normal approximate closing dates of 47–59 weeks for the Greyhound (Smith & Allcock, 1960), with other publications ranging between 45 and 81 weeks of age. The dental and bone morphology therefore would put this dog at almost complete skeletal maturity, roughly between 9 and 24 months of age. There is bone reaction at the ventral endplates of the lumbosacral joint, consistent with early spondylosis deformans, a degenerative remodeling and ventral bridging of intervertebral disk spaces that is ubiquitous in modern day dogs and usually without

clinical consequences. There is no evidence of bony reaction at any of the bone fragment margins, hence these are unlikely old injuries. Most likely they represent post mortem related damage, but acute trauma cannot be ruled out.

4.3 | Wider context of Romano-British dogs

The Warmington dog is of similar type to animals previously described from less complete material found at Thistleton (Baxter, n.d.) and Vindolanda (Bennett & Timm, 2016) typified by long and lightly built limb bones. These animals were coursers analogous to the modern Greyhound and Ibizan hound. Frequently depicted on Roman mosaics hunting hares and rabbits they correspond to dogs referred to as Laconian or Celtic hounds. The Celtic hound, or *vertragus*, is described by Arrian as exceptionally fast and adept at catching hares by speed (Brewer, Clark, & Phillips, 2001).

Although the Warmington dog's skeleton reveals size and shape information, and gives us clues as to its main suitability and use, it does not reveal major characteristics that determined its appearance, such as its pelage or how it carried its tail and ears. Roman hounds, as we know from contemporaneous illustrations and mosaics, were quite variable in these respects. In order not to suggest any resemblance to a modern pedigree breed, we present various random combinations of those breed-defining, external features to illustrate how they can change the superficial appearances of dogs (Figure 8).

5 | CONCLUSION

Although the Warmington Roman dog shares some morphological similarities with modern sight hounds, we do not claim that it was an ancestor of this or any other modern dog group. Evidence of such would necessitate analysis of its DNA. Rather, we speculate that morphological convergence between these dogs is a function of their bred purpose, the need for hunting by speed.

ORCID
Jeffrey J. Schoenebeck https://orcid.org/0000-0003-4964-2138
Tobias Schwarz https://orcid.org/0000-0001-8412-573X

REFERENCES

Baxter, I. L. (n.d.) *A re-examination of the Thistleton Canids*. Retrieved from http://alexandriaarchive.org/bonecommons/archive/files/a-re-examination-of-the-thistleton-canids_6025e08cf4.pdf

Bennett, D., Cambell, G., & Timm, R. M. (2016). The dogs of Roman Vindolanda, Part I: Morphometric techniques useful in differentiating domestic and wild canids. *Archaeofauna*, *25*, 1–31.

Bennett, D., & Timm, R. M. (2016). The dogs of Roman Vindolanda, Part II: Time-stratigraphic occurrence, ethnographic comparisons, and biotype reconstruction. *Archaeofauna*, *25*, 107–126.

Botigué, L. R., Song, S., Scheu, A., Gopalan, S., Pendleton, A. L., Oetjens, M., … Veeramah, K. R. (2017). Ancient European dog genomes reveal continuity since the Early Neolithic. *Nature Communications*, *8*, 16082.

Boyko, A. R., Quignon, P., Li, L., Schoenebeck, J. J., Degenhardt, J. D., Lohmueller, K. E., … Ostrander, E. A. (2010). A simple genetic architecture underlies morphological variation in dogs. *PLoS Biology*, *8*, e1000451–e1000450.

Brewer, D. J., Clark, T., & Phillips, A. (2001). *Dogs in antiquity: Anubis to cerberus: The origins of the domestic dog*. Warminster, England: Aris & Phillips.

Chase, K., Carrier, D. R., Adler, F. R., Jarvik, T., Ostrander, E. A., Lorentzen, T. D., & Lark, K. G. (2002). Genetic basis for systems of skeletal quantitative traits: Principal component analysis of the canid skeleton. *Proceedings of the National Academy of Sciences*, *99*, 9930–9935.

Drake, A. G. (2011). Dispelling dog dogma: An investigation of heterochrony in dogs using 3D geometric morphometric analysis of skull shape. *Evolution & Development*, *13*, 204–213.

Drake, A. G., & Klingenberg, C. P. (2010). Large-scale diversification of skull shape in domestic dogs: Disparity and modularity. *The American Naturalist*, *175*, 289–301.

Evin, A., Souter, T., Hulme-Beaman, A., Ameen, C., Allen, R., Viacava, P., … Dobney, K. (2016). The use of close-range photogrammetry in zooarchaeology: Creating accurate 3D models of wolf crania to study dog domestication. *JASREP*, *9*, 87–93.

Frantz, L. A. F., Mullin, V. E., Pionnier-Capitan, M., Lebrasseur, O., Ollivier, M., Perri, A., … Larson, G. (2016). Genomic and archaeological evidence suggest a dual origin of domestic dogs. *Science*, *352*, 1228–1231.

Freedman, A. H., Gronau, I., Schweizer, R. M., Ortega-Del Vecchyo, D., Han, E., Silva, P. M., … Novembre, J. (2014). Genome sequencing highlights the dynamic early history of dogs. *PLoS Genetics*, *10*, e1004016.

Geiger, M., & Haussman, S. (2016). Cranial suture closure in domestic dog breeds and its relationships to skull morphology. *The Anatomical Record*, *299*, 412–420.

Harcourt, R. A. (1974). The dog in prehistoric and early historic Britain. *Journal of Archaeological Science*, *1*, 151–175.

Jiang, X., Iseki, S., Maxson, R. E., Sucov, H. M., & Morriss-Kay, G. M. (2002). Tissue origins and interactions in the mammalian skull vault. *Developmental Biology*, *241*, 106–116.

Klingenberg, C. P. (2016). Size, shape, and form: Concepts of allometry in geometric morphometrics. *Development Genes and Evolution*, *226*, 113–137.

Lobell, J. A., Powell, E. (2010). *Dogs of Roman Britain. Archaeology*. 63. Retrieved from https://archive.archaeology.org/1009/dogs/romanbrits.html

Lüps, P. (1973). Biometrische Untersuchungen an der Schädelbasis des Haushundes. *Zoologischer Anzeiger*, *192*, 383–413.

Marchant, T. W., Johnson, E. J., McTeir, L., Johnson, C. I., Gow, A., Liuti, T., ... Schoenebeck, J. J. (2017). Canine brachycephaly is associated with a retrotransposon-mediated missplicing of SMOC2. *Current Biology*, *27*, 1573–1584.e6.

McBratney-Owen, B., Iseki, S., Bamforth, S. D., Olsen, B. R., & Morriss-Kay, G. M. (2008). Development and tissue origins of the mammalian cranial base. *Developmental Biology*, *322*, 121–132.

Mihaljević, M., Kramer, M., & Gomerčić, H. (Eds.). (2009). *CT-und MRT-Atlas*. Stuttgart, Germany: Parey Verlag.

Mosimann, J. E. (1970). Size allometry: Size and shape variables with characterizations of the lognormal and generalized gamma distributions. *Journal of the American Statistical Association*, *65*, 930–945.

Noden, D. M., & Trainor, P. A. (2005). Relations and interactions between cranial mesoderm and neural crest populations. *Journal of Anatomy*, *207*, 575–601.

Nussbaumer, M. (1982). Über die Variabilität der dorso-basalen Schädelknickungen bei Haushunden. *Zoologischer Anzeiger*, *209*, 1–32.

Parker, H. G., vonHoldt, B. M., Quignon, P., Margulies, E. H., Shao, S., Mosher, D. S., ... Ostrander, E. A. (2009). An expressed fgf4 retrogene is associated with breed-defining chondrodysplasia in domestic dogs. *Science*, *325*, 995–998.

Parr, W. C. H., Wilson, L. A. B., Wroe, S., Colman, N. J., Crowther, M. S., & Letnic, M. (2016). Cranial shape and the modularity of hybridization in dingoes and dogs: Hybridization does not spell the end for native morphology. *Evolutionary Biology*, *43*, 171–187.

Pionnier-Capitan, M., Bemilli, C., Bodu, P., Célérier, G., Ferrié, J.-G., Fosse, P., ... Vigne, J.-D. (2011). New evidence for Upper Palaeolithic small domestic dogs in South-Western Europe. *Journal of Archaeological Science*, *38*, 2123–2140.

Ryan, J. M., Fraga-Manteiga, E., Schwarz, T., & Clements, D. N. (2013). Unilateral synostosis of the zygomaticotemporal suture associated with mandibular coronoid process impingement in a dog. *Veterinary and Comparative Orthopaedics and Traumatology*, *26*, 421–424.

Schoenebeck, J. J., Hutchinson, S. A., Byers, A., Beale, H. C., Carrington, B., Faden, D. L., ... Ostrander, E. A. (2012). Variation of BMP3 contributes to dog breed skull diversity. *PLoS Genetics*, *8*, e1002849.

Saunders, J., & Schwarz, T. (2011). Principles of CT Image Interpretation. In: Schwarz, T., & Saunders, J. (Eds.) *Veterinary Computed Tomography*. West Sussex, England: Wiley-Blackwell.

Selba, M. C., Oechtering, G. U., Heng, H. G., & DeLeon, V. B. (2019). The impact of selection for facial reduction in dogs: Geometric morphometric analysis of canine cranial shape. *The Anatomical Record*, *51*, 904.

Skoglund, P., Ersmark, E., Palkopoulou, E., & Dalén, L. (2015). Ancient wolf genome reveals an early divergence of domestic dog ancestors and admixture into high-latitude breeds. *Current Biology*, *25*, 1515–1519.

Smith, K. (2005). In M. Aldhouse-Green (Ed.), *Domesticated dogs in the art and archaeology of iron age and Roman Britain*. Newport, England: University of Wales.

Smith, R. N., & Allcock, J. (1960). Epiphysial fusion in the greyhound. *The Veterinary Record*, *72*, 75–79.

Sutter, N. B., Bustamante, C. D., Chase, K., Gray, M. M., Zhao, K., Zhu, L., ... Ostrander, E. A. (2007). A single IGF1 allele is a major determinant of small size in dogs. *Science*, *316*, 112–115.

von den Driesch, A. (1976). A guide to the measurement of animal bones from archaeological sites. *Harvard University: Peabody Museum Bulletins*, *1*, 1–137.

Wang, G.-D., Zhai, W., Yang, H.-C., Fan, R.-X., Cao, X., Zhong, L., ... Zhang, Y. P. (2013). The genomics of selection in dogs and the parallel evolution between dogs and humans. *Nature Communications*, *4*, 1860.

Wayne, R. (1986). Cranial morphology of domestic and wild canids: The influence of development on morphological change. *Evolution*, *40*, 243–261.

SUPPORTING INFORMATION

Additional supporting information may be found online in the Supporting Information section at the end of this article.